Strain gradients and normal stresses in textured Mo thin films

S. G. Malhotra[a)]
Department of Materials Science and Engineering, University of Michigan, Ann Arbor, Michigan 48109-2136

Z. U. Rek
Standford Synchrotron Radiation Laboratory, Stanford, California 94395

S. M. Yalisove and J. C. Bilello
Department of Materials Science and Engineering, University of Michigan, Ann Arbor, Michigan 48109-2136

(Received 12 July 1996; accepted 15 November 1996)

The high-resolution x-ray-diffraction technique was used to explore strain variations in sputtered Mo films with thicknesses of 170, 260, and 800 nm that possess a (110) out-of-plane texture. The strains in crystallographic planes perpendicular to the surface of each film were found to be nominally constant and compressive at all x-ray penetration depths. Near the surface of each film, the inclined-plane strains were compressive, and then relaxed as the penetration depths approached each entire film thickness. The strain tensor in a laboratory reference frame for each film, as a function of penetration depth, revealed that the normal strain ϵ_{zz} was tensile near the surface of each film, and then relaxed to a nominally constant value as the penetration depths approached the entire film thickness. The penetration depth over which the normal strain decayed to a nominally constant value increased as the total film thickness increased. A consequence of the large normal strains near the free surface of each film is that the corresponding normal stresses were nonzero. © *1997 American Vacuum Society.* [S0734-2101(97)01102-0]

I. INTRODUCTION

Thin metal films that grow with a preferred crystallographic orientation are used for a variety of technologically important applications. For example, a strong and tough multiscalar multilayer primarily composed of Mo, which is being developed for use as a high-temperature coating, develops a (110) in-plane texture.[1,2] Mo films that develop a (110) out-of-plane texture are also used for x-ray mirrors[3] and as the bottom electrode in solar cells.[4] The development of excessive residual strains during the growth of these films can affect the mechanical, optical, and electrical properties of the film. Therefore, an understanding of the interplay between stress, strain, and microstructure is important for the production of reliable thin-film structures.

Several investigators have noted a correlation between the microstructure in Mo and other thin films and the average stress throughout the entire film thickness.[5–7] For example, it has been observed that compressively stressed films have a relatively low density of voids at the column boundaries. Conversely, films that exhibit an average tensile stress have a high degree of voiding at the boundaries of the columns; however, it has been shown that microstructural features change during film growth.[6,8–11] In physically vapor deposited films, the grains near the substrate tend to be small and equiaxed. With increasing film thickness the films become more crystallographically textured, the average grain size increases, and the void density at the grain boundaries increases. Thus, the use of a depth sensitive technique to probe the strain can lead to a better understanding of the relationship between the strain and microstructure.

The depth of penetration into a material can be controlled when conducting direct measurements of interplanar spacings with x-ray diffraction in a grazing incidence geometry, because one can use the phenomenon of total external reflection of the incident x-ray beam.[12–14] This is in contrast to substrate curvature methods[15–24] and the $\sin^2\psi$ technique[25–27] which can only determine the average stress throughout the entire film thickness. A high-resolution x-ray-diffraction (HRXRD) technique, which combines two grazing incidence geometries, was recently used to study polycrystalline Mo films less than 100 nm thick.[28] It was found that the strains parallel to the film surfaces were constant and isotropic as a function of penetration depth, but also that the strain normal to the film surfaces varied as a function of penetration depth. Additionally, the normal strain was tensile near the free surface of the films. A correlation to the microstructure was not made.

The goal of the present study was to explore strain variations in thicker Mo films that are beginning to develop a preferred out-of-plane growth direction, and begin to correlate these results with microstructural features. Thus, the HRXRD technique was used to determine the depth dependence of the strain in Mo films that are 170, 270, and 800 nm thick, which possess a (110) out-of-plane texture.

[a)]Presently at International Business Machines Corp., Semiconductor Research & Development Center, 1580 Rte. 52, Hopewell Junction, NY 12533.

TABLE I. List of diffraction peaks collected at each penetration depth from the free surface of the 170-nm-thick Mo film.

Penetration depth (nm)	Peaks collected in symmetric geometry	Peaks collected in asymmetric geometry
5, 10	{110}, {200}, {211}, {220}, {310}, {321}	{110}, {200}, {211}
25, 60, 110	{110}, {200}, {220}, {310}, {222}, {321}, {400}	{110}, {200}, {211}
170	{110}, {200}, {211}, {220}, {310}, {222}, {321}, {400}	{110}, {200}, {211}

II. EXPERIMENTAL PROCEDURES

A. Sample preparation

Molybdenum films, with thicknesses of 170±8.5, 270 ±13.5, and 800±40 nm, were deposited from a 99.95% pure Mo target onto 75-mm-diam Si(100) wafers by direct current planar magnetron sputtering. The wafers were in the ''as-received'' condition, with a native oxide coating. The sputtering occurred without significant heating of the substrates. The sputtering power was 308 W (~8 nm/min deposition rate) and the chamber was pumped to a base pressure $\sim 6\times 10^{-6}$ Torr. The chamber was then backfilled with Ar and maintained at a pressure of $\sim 1\times 10^{-3}$ Torr. The samples were mounted face down 5 in. above the sputter source in a horizontal platen which rotated at 20 rpm. The target was presputtered onto the shutter for at least 3 min to prevent oxides or contaminants from being sputtered onto the wafers.

B. Measurement

The present HRXRD experiments were conducted at the Stanford Synchrotron Radiation Laboratory (SSRL) under standard conditions (3 GeV and 100 mA at fill) on the eight-pole focused wiggler station BL 7−2. A Si(111) double-crystal monochromator was used to select the incident x-ray wavelength of 0.124 nm (10 keV) from the continuous spectrum. The horizontal and vertical divergence of the beam on BL 7−2 is 3 and 0.2 mrad, respectively. Slits 1×1 mm^2 were used for the incoming beam, and 1 mrad Soller slits were used for the diffracted beam to limit vertical divergence. The signal was detected with a Ge detector. The samples were mounted on an automated Huber four-circle goniometer. The dedicated BL 7−2 computer was used to control the goniometer motions, the shutter, and the photon counting. The experiments were conducted in the ''dose'' mode by putting a scintillation counter in the path of the incident beam, because the current in the synchrotron ring decreased linearly with time. The need for a high-brightness source such as a synchrotron for precision strain measurements in thin films was demonstrated previously.[28]

The HRXRD technique uses both the symmetric and asymmetric grazing incidence geometries[29] to collect the diffraction data, so that crystallographic planes with a variety of orientations can be probed. The diffraction condition can be satisfied for crystallographic planes which are nearly perpendicular to the sample surface in the symmetric configuration, whereas the diffraction condition can be satisfied for planes which are inclined to the sample surface in the asymmetric configuration. The x-ray penetration depths were varied by changing the angle of the incoming x-ray near the critical angle for total external reflection of 0.34°.[30] The diffraction peaks collected in the symmetric and asymmetric geometries, at each penetration depth for each film, are shown in Tables I, II, and III.

TABLE II. List of diffraction peaks collected at each penetration depth from the free surface of the 260-nm-thick Mo film.

Penetration depth (nm)	Peaks collected in symmetric geometry	Peaks collected in asymmetric geometry
5, 10, 65, 125, 260	{110}, {200}, {211}, {220}, {310}, {321}	{110}, {200}, {211}

The nature and degree of the texture in the Mo films were measured from reflection x-ray pole figures. The pole figures were obtained from a Rigaku texture diffractometer configured in the Schultz geometry,[31] which was attached to a Rigaku Rotaflex equipped with a 12 kW Cu rotating anode source (0.154 nm radiation). Pole figures for the (110), (200), and (211) poles were collected for all of the films, as well as for a random polycrystalline Mo standard. The Mo standard was prepared by powder pressing and sintering, had an average grain size of >10 μm, and was thick enough to absorb ~100% of the incident rays. The degree of the texture the Mo films was quantified by a ''times random'' approach, which is elucidated elsewhere.[8]

The average biaxial stresses in the films were determined by a macroscopic substrate curvature technique, double-crystal diffraction topography (DCDT). The technique is based on the observation that, for a bent single crystal substrate (Si for this work) which is illuminated with highly parallel and monochromatic x rays, only that portion of the crystal lattice that is in the Bragg condition will create a topographic image in an x-ray photographic film detector.[18–20] By initially capturing the topographic image of the portion of the sample in the Bragg condition, and then rotating the sample about an axis perpendicular to the plane of diffraction and exposing the film again, a series of bands will form on the film. From this information, the substrate curvature can be calculated. If the curvature of the substrate is determined before and after the film deposition, the average

TABLE III. List of diffraction peaks collected at each penetration depth from the free surface of the 800-nm-thick Mo film.

Penetration depth (nm)	Peaks collected in symmetric geometry	Peaks collected in asymmetric geometry
5, 10, 50, 120, 200	{110}, {200}, {211}, {310}, {222}, {321}, {400}	{110}, {200}, {211}, {310}
105, 110, 130, 260, 290		{110}, {200}, {211}, {310}

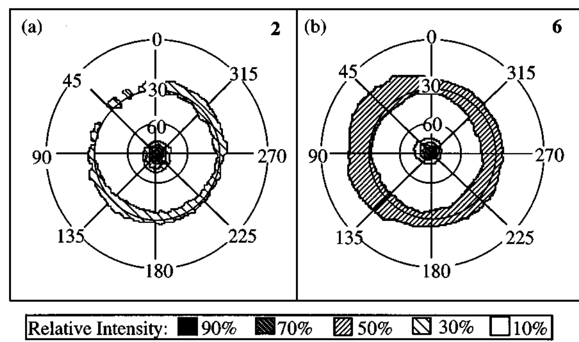

FIG. 1. (110) pole figures for (a) 260 nm and (b) 800 nm Mo films. In all of the pole figures the sample normal is parallel to the page normal, and the times random values are indicated in the upper right-hand side. Relative intensity refers to the percentage of the maximum times random diffraction intensity in each pole figure. The times random value for the 260 nm film was also 2, so the pole figure was not shown for brevity. The intensity concentrations coaxial with the sample normal and 60° away from it indicate a preferred (110) growth direction in these films.

biaxial stress throughout the entire film thickness can be determined using the modified Stoney equation.[21–23] A detailed description of the DCDT apparatus used for this study is contained in a previous publication.[24]

III. RESULTS

A (110) pole figure for the 260 and 800 nm films is shown in Fig. 1. This two-dimensional pole figure illustrates the location of (110) planes, in three-dimensional space, as a function of the inclination angle α and the azimuthal angle β. The presence of intensity concentrations near the α angles of 0° and 30°, and symmetry of the diffraction intensity at all β angles, indicates the presence of a (110) out-of-plane texture in both films. The (200) and (211) pole figures support this conclusion, but were not shown for brevity. [As shown in Fig. 1 the maximum times random values for the 170, 260, and 800 nm films when compared to a polycrystalline solid standard were 2, 2, and 6, respectively, indicating the presence of a weak (110) out-of-plane texture in each film.]

The diffraction data were corrected for Lorentz polarization and absorption and fit with a Voigt or Gaussian function to determine the location of each peak 2θ. This was then used to determine the interplanar spacings for each $\{hkl\}$ family of planes d_{hkl} from Bragg's law and the strain was calculated using $\epsilon_{hkl}=(d_{hkl}-d_0)/d_0$. Because of the difficulties involved in making a strain-free refractory metal film standard, a strain-free lanthanum hexaboride powder standard (NIST SRM 660) was used to detect any systematic offset during the experiment. The Joint Committee for Powder Diffraction Standards (JCPDS) d_0 values for Mo were then corrected for this offset and used for the strain calculations. The resulting strains obtained in the symmetric geometry are shown in Fig. 2, and the strains obtained in the asymmetric geometry are shown in Fig. 3.

The strain tensors for all of the penetration depths in each film were calculated using the least squares methodology developed by Imura, Weissmann, and Slade.[32] The laboratory frame of reference used for the tensor calculations is shown in Fig. 4. The x, y, and z axes in the laboratory frame were defined by considering the orientation of the plane of diffraction in the asymmetric geometry. The diffraction plane contains the incoming x ray $\mathbf{k_0}$, the diffracted x ray $\mathbf{k}$, and the sample normal, $\mathbf{n}$. Thus, the sample normal defined the z axis, the perpendicular component to the diffraction plane defined the x axis, and the cross product of x and z defined the y axis. The Si[110] direction is parallel to the y axis, and this direction was placed perpendicular to the axis of rotation, and parallel to the tangent of the platen, during sputter deposition. Once defined in the laboratory reference frame, all strain displacement vectors were used to solve for the six unknowns in the strain tensor. The strain eigenvalues and eigenvectors were then calculated for each symmetric strain tensor using the approach outlined by Nye.[33] The normal components of the strain tensor are shown in Fig. 5. The strain eigenvalues were converted to stresses using Hooke's law and the bulk elastic constants E and ν.[34] The degree of texture in the films was not significant enough to warrant the use of the single-crystal elastic constants.

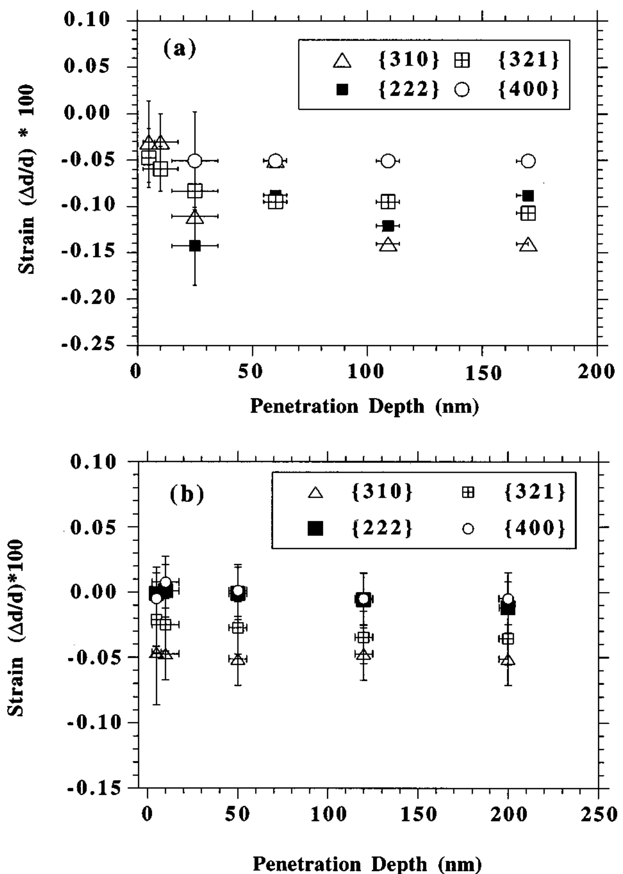

FIG. 2. Strains in planes perpendicular to the sample surface, obtained in the symmetric grazing incidence geometry, for (a) 170 nm and (b) 800 nm Mo films. There is not a significant strain gradient through the thickness of either film. The 260 nm film displayed the same trend and was not shown for brevity.

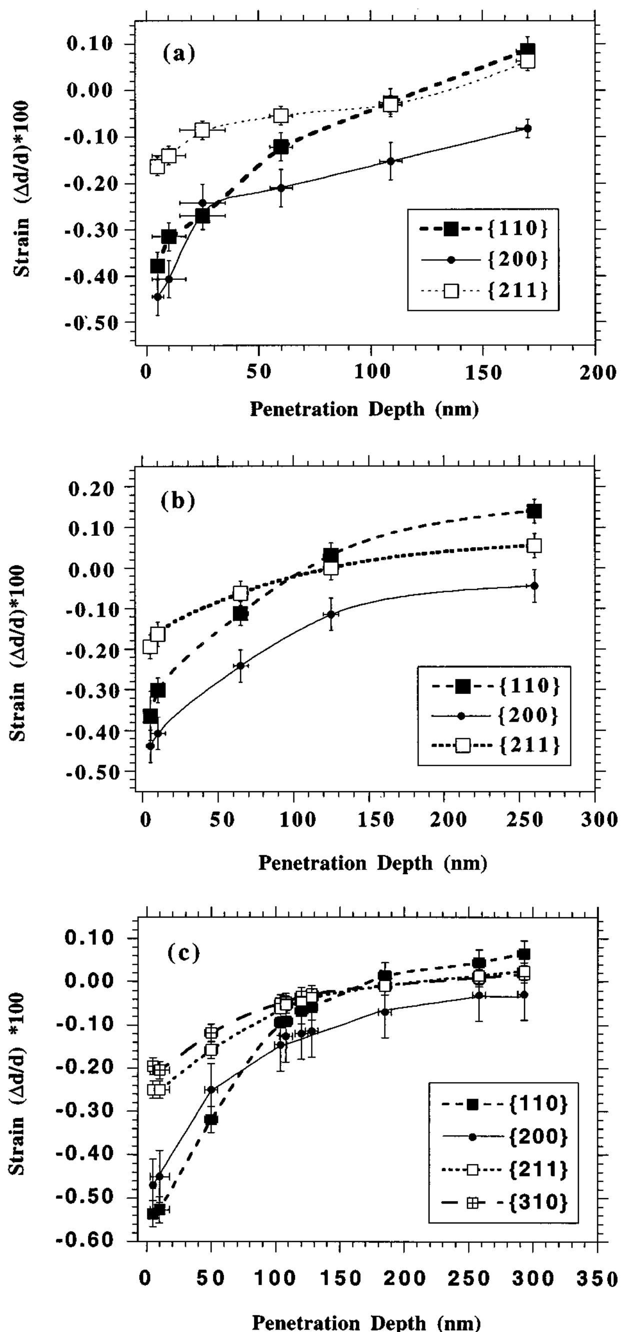

FIG. 3. Strains in planes inclined with respect to the sample surface, obtained in asymmetric grazing incidence geometry, for (a) 170 nm, (b) 260 nm, and (c) 800 nm films. There is a strain gradient in these planes, which decreases in magnitude as the penetration depth from the free surface increases.

IV. DISCUSSION

The microstructural evolution of Mo films dynamically sputter deposited onto the native oxide of Si(100), in 10 mTorr Ar, at a rate of 34 nm/min, was reported in a previous publication.[8] This study combined transmission electron microscopy (TEM) and x-ray-diffraction to study the development of out-of-plane and in-plane texture in Mo films sputtered onto moving substrates as a function of film thickness.

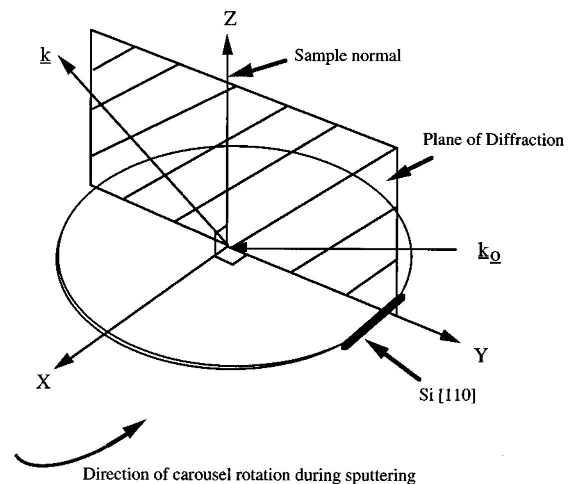

FIG. 4. Schematic of laboratory axis system used for strain eigenvalue and eigenvector calculations. The sample normal, incident x ray, $\mathbf{k}_0$ and diffracted x-ray $\mathbf{k}$ comprise the diffraction plane. The sample normal forms the z axis, the perpendicular to the diffraction plane the x axis, and the cross product of the x and z axes forms the y axis.

The results of that study were used to deposit Mo films with the degree of texture desired for the present work, and are summarized as follows. X-ray pole figure analysis showed that films with a thickness below 80 nm were polycrystalline, and that films with a thickness of 200 nm developed a {110} out-of-plane texture. In films with a thickness above 200 nm, the intensity of the {110} out-of-plane texture continued to increase with film thickness. A twofold symmetry in the diffraction intensity began to appear in 1 μm films, indicating the development of a {110} in-plane texture. The {110} in-plane alignment became pronounced once the films reached a thickness of 2 μm. The 170, 260, and 800 nm films used for this work had a {110} out-of-plane texture, as illustrated in Fig. 1, with maximum times random values equal to 2, 2, and 6. The alignment of the planes in the {110} growth direction is expected in bcc thin films because the {110} planes have the highest planar packing density, and a minimum surface free energy.[35] At small film thicknesses, where the surface-to-volume ratio in the film is high, minimization of the surface free energy will dominate thin-film growth.[36–39]

The strains for higher-order planes perpendicular to the sample surface as a function of penetration depth are shown in Fig. 2 for the 170 and 800 nm films, which is representative of the data for the 260 nm film. The entire thickness of the 800 nm film could not be penetrated in the symmetric grazing incidence geometry, so data were collected for the top 200 nm only. The strains display a negligible gradient and maintain a value of approximately −0.10% for the 170 nm film, and −0.03% for the 800 nm film. A negligible strain gradient was also found for thin polycrystalline Mo films[28] and highly textured Al alloy films.[29] This indicates that the strain state remains isotropic in the plane of growth, even as a preferred out-of-plane growth direction forms.

A significant strain gradient was identified for crystallographic planes inclined to the sample surface in both the 170,

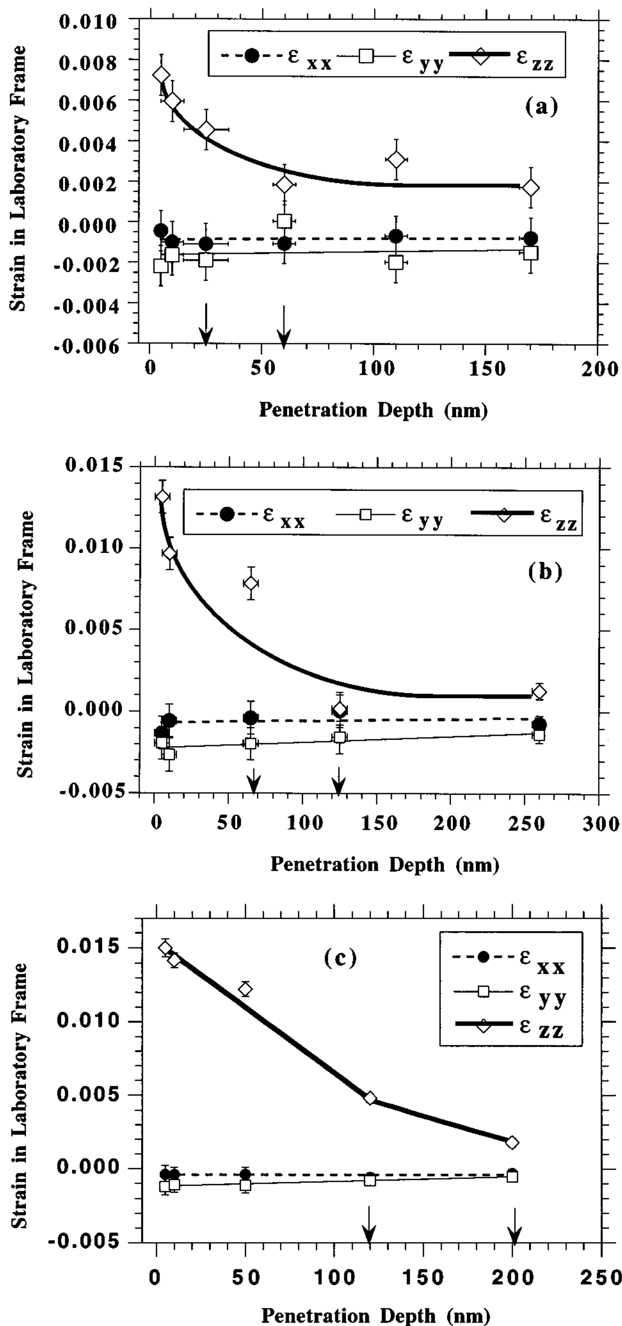

FIG. 5. Normal components of strain tensor as a function of penetration depth for (a) 170, (b) 260, and (c) 800 nm Mo films. The normal strain ϵ_{zz} is tensile near the free surface of each film, and then decays to a nominally constant value. The arrows indicate the area in which the normal strain decays to a constant value.

260, and 800 nm films, as shown in Figs. 3(a), 3(b), and 3(c), respectively. The data were collected at increasing penetration depths for the 800 nm film until the strains relaxed to a nominally constant value. A correction for the refractive index was taken in to consideration.[40] The strains in the {110}, {200}, and {211} planes were compressive near the free surfaces (-0.20% to -0.50%) and then become more tensile, at about the same rate. When the entire film thicknesses are penetrated, the strains were between $+0.10\%$ and -0.10%.

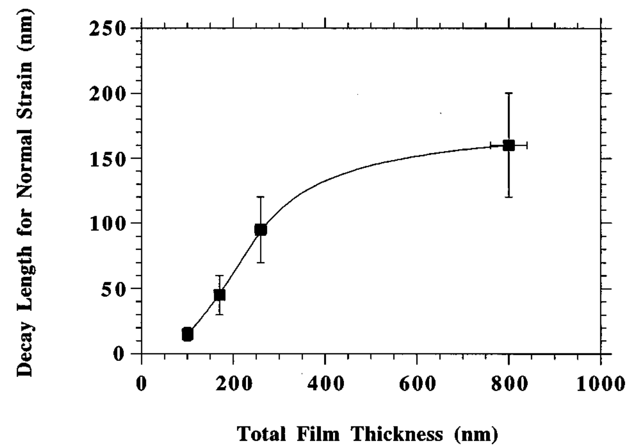

FIG. 6. The decay length for the normal strain ϵ_{zz} as a function of total film thickness. The line is intended as a guide for the eye. The increase in the decay length with film thickness increases may be related to microstructural features such as grain size and surface roughness, which also increase as film thickness increases.

Although inclined-plane strains as a function of penetration depth in thin films have not been widely studied, Ballard, *et al.* recently reported that the *d* spacing of (321) planes in a 1 μm Mo film, obtained in the asymmetric grazing incidence geometry, varied as a function of penetration depth.[41]

The strain tensor in the laboratory reference frame for the 170, 260, and 800 nm films are shown in Figs. 5(a)–5(c), respectively. The strains along the x and y directions in the laboratory frame, ϵ_{xx} and ϵ_{yy}, remain relatively constant and compressive at each penetration depth, with magnitudes between -1×10^{-3} and -5×10^{-3}. This is in agreement with the strain information obtained from the symmetric grazing incidence geometry in Fig. 2, because both are indicating strains in planes perpendicular to the film surface. On the other hand, the normal component in the laboratory frame, ϵ_{zz} varies as a function of penetration depth in each film. For the shallowest penetration depth, 5 nm, the normal strain reaches $+7\times10^{-3}$ for the 170 nm film, $+13\times10^{-3}$ for the 260 nm film, and $+15\times10^{-3}$ for the 800 nm film. The normal strain ϵ_{zz} then smoothly decreases to a value of about $+1\times10^{-3}$ for each film. The arrows in the figures indicates the area where the normal strain ϵ_{zz} decays to a value representative of the entire film thickness; this is discussed in detail below.

The origin of the strain profiles in the sputtered Mo films may be related to several factors, including voids,[6] oxygen or argon impurities,[42–45] and crystallographic flaws.[46] The data in Fig. 6 may give some insight into the factors influencing the strain gradients. Figure 6 shows the penetration depth where the normal strain ϵ_{zz} decays to a nominally constant value (indicated by the arrows in Fig. 5, and in previously published data[28] for a 100 nm Mo film) as a function of total film thickness. This distance is referred to as the decay length for the normal strain. As shown in Fig. 6, the decay length increases as the total film thickness increases. The error bars indicate the uncertainty in the decay length due to the density of the data points in Fig. 5. The trend in Fig. 6

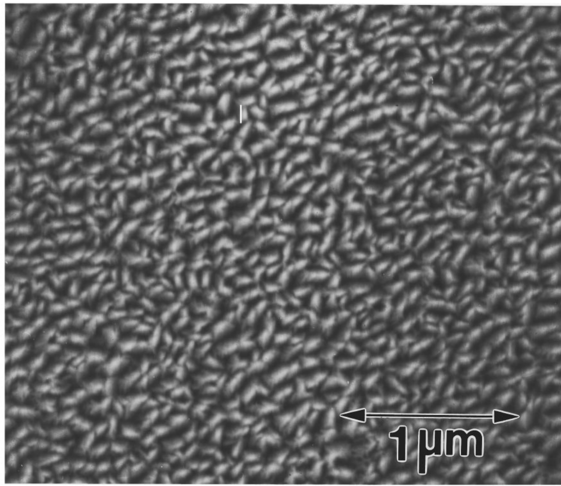

FIG. 7. Plan-view micrograph of 800 nm Mo film taken on the scanning electron microscope which illustrates significant surface roughness. The grains are evolving into a zone 2 microstructure, which is characterized by highly oriented columnar grains and faceted surfaces.

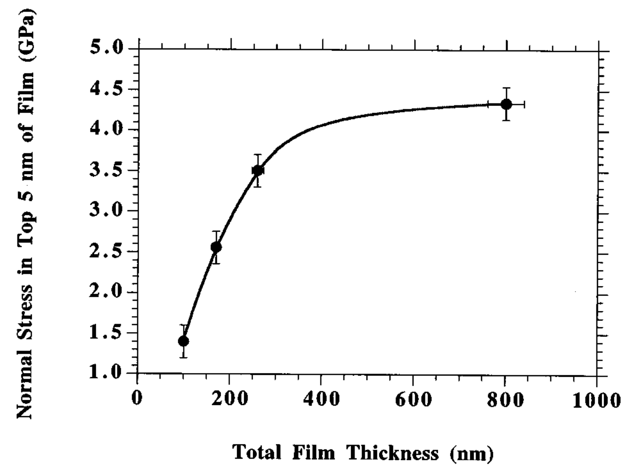

FIG. 8. Magnitude of the normal stress σ_{zz} in the top 5 nm of several Mo films as a function of total film thickness. The line is intended as a guide for the eye. The stress was calculated using linear elasticity and bulk elastic constants ($E_{\mathrm{Mo}}=324$ GPa and $\nu_{\mathrm{Mo}}=0.293$). Because the normal stress near a free surface must be zero due to mechanical equilibrium, this result would imply that the surface of a thin film cannot be considered to be a perfect linear elastic solid.

may be related to an increase in the grain size and/or the surface roughness with film thickness. A previous publication showed a nearly linear increase in the grain size as a function of Mo film thickness for films between 5 and 80 nm in thickness that were magnetron sputtered under similar conditions.[11] Also, the plan-view scanning electron micrograph shown in Fig. 7 for the 800 nm film shows substantial surface roughness. A more detailed study of the grain sizes and surface roughness, with atomic force microscopy, will be needed to correlate these microstructural features to the strain gradients. The determination of the relevant microstructural feature would then shed light on possible mechanisms for the strain generation.

One consequence of the large normal strains ϵ_{zz} near the free surface of each film is that the corresponding normal stresses σ_{zz} are nonzero. The normal stress for the top 5 nm of each film was calculated using linear elasticity and the bulk elastic constants E and ν, and is shown in Fig. 8. The value of σ_{zz} for the top 5 nm of each film increased with total film thickness. The values of the normal stress over each entire film thickness were also determined, and were nominally zero, as expected from mechanical equilibrium. A plausible explanation for the near-surface stress behavior is that the surface normal direction no longer corresponds to the normal direction in the laboratory reference frame due to surface roughness. The analysis of the normal stress near the surface of thin films has not been widespread because it is difficult to obtain. Common stress measurement techniques, such as substrate curvature and $\sin^2 \psi$ methods, determine the stresses over the entire film thickness and assume a biaxial stress state *a priori*.[15–27] Depth sensitive techniques, such as grazing incidence x-ray scattering (GIXS), are generally used to profile in-plane strains as a function of x-ray penetration depth.[29,47,48] The symmetric $\theta-2\theta$ scattering geometry can be used to determine the average normal strain only.[49,50] However, the recently developed HRXRD technique,[28] used for this study, can yield the variation of the normal stresses and strains as a function of x-ray penetration depth for penetration depths as shallow as 5 nm from the free surface.

The determination of the magnitudes of the errors in Figs. 2, 3, and 5 was discussed in detail in a previous publication.[28] The error in the penetration depth depends on the uncertainty in the incident angle and how close the incident angle is to the critical angle. Very near the critical angle the uncertainty in the penetration depth is greatest (≈30 nm). The uncertainty in the crystallographic strains arose from both systematic and random errors that occurred during the experiments. Great care was exercised to minimize systematic errors from instrument misalignment, specimen displacement, and beam divergence. Also, the random counting errors were minimized by taking the following three precautions:

(1) The experiments were operated in the count mode, and at least 100 000 counts were collected from the incident beam for each data point;
(2) the data were collected in angular increments of 1×10^{-2}–1.5×10^{-2} deg; and
(3) many of the diffraction peaks were collected multiple times.

The magnitude of the systematic error in the diffraction experiments was evaluated by a careful analysis of the LaB_6 standard data. The magnitude of the random errors in the crystallographic strains was determined by differentiating Bragg's law, and was equal to a maximum in $\Delta d/d$ of $\pm5\times10^{-4}$ for the low signal-to-noise higher-order peaks. The maximum errors in the strain eigenvalues were determined using the approach described by Witte, Winholtz, and Neal,[51] and a more detailed analysis of the LaB_6 standard data, and were also $\pm5\times10^{-4}$.

TABLE IV. Comparison of average biaxial stresses through the entire film thickness determined by double-crystal diffraction topography (DCDT) and the high-resolution x-ray-diffraction method (HRXRD).

Film thickness (nm)	Stress (GPa)	
	DCDT	HRXRD
170	−0.350±0.070	−0.800±0.100
260	−0.410±0.050	−0.570±0.100

Finally, a comparison of the average stresses obtained from this high-resolution diffraction technique is consistent with the average residual stress measurements with DCDT on these same films. The magnitude of the biaxial stress in the 170 and 260 nm films obtained from DCDT and the average of σ_{xx} and σ_{yy}, for the entire film thickness, determined with the current technique is shown in Table IV.

V. CONCLUSIONS

Strain variations, as a function of x-ray penetration depth, were reported for 170, 260, and 800 nm Mo films. These films have an (110) out-of-plane texture, or (110) preferred growth direction, with times random values between 2 and 6. It was observed that the strains in crystallographic planes that are perpendicular to the sample surface remained relatively constant throughout the thickness of the films. On the other hand, the strains in crystallographic planes that are inclined to the sample surface displayed a large variation as a function of x-ray penetration depth. The strains were compressive near the free surface of each film (from −0.20% to −0.55%), and then relaxed as the penetration depths approached the entire film thickness.

The strain eigenvectors rotated onto the laboratory reference frame for each film, as a function of penetration depth, revealed the variation of the azimuthal strains ϵ_{xx} and ϵ_{yy} and the normal strain ϵ_{zz} throughout each film thickness. In each case, ϵ_{xx} and ϵ_{yy} maintained a nominally constant and compressive value as a function of penetration depth. The normal strain ϵ_{zz} was tensile near the free surface and then decreased to a nominally constant value. The maximum normal strain and the penetration depth over which the normal strain decayed to a constant value differed for each film. For the 170 nm film the maximum normal strain was $+7\times10^{-3}$ and the normal strain decayed for a penetration depth between 25 and 60 nm; for the 260 nm film the maximum normal strain was $+13\times10^{-3}$ and the normal strain decayed for a penetration depth between 65 and 125 nm; for the 800 nm film the maximum normal strain was $+15\times10^{-3}$ and the normal strain decayed for a penetration depth between 120 and 200 nm. As a result of the large normal strains near the free surface of each film, the corresponding normal stresses near the free surface of each film were nonzero. A plausible explanation for this behavior is the existence of a modulus defect, which can arise from impurities or a void network. This finding implies that the surface of a thin film is not a perfect elastic solid, and that the use of the bulk elastic constants E and V to calculate the stresses is not correct.

ACKNOWLEDGMENTS

This work was supported by the USARO and ARPA under Contract No. DAAH04-95-1-0120. The synchrotron work was conducted at the Stanford Synchrotron Radiation Laboratory (SSRL), funded by the U.S. Department of Enorsy. The authors wish to thank G. Brooks from the University of Michigan Department of Materials Science and Engineering, J. Kulman at the University of Michigan Solid State Electronics Laboratory, and Dr. S. Brennan at SSRL.

[1]M. Vill, D. P. Adams, S. M. Yalisove, and J. C. Bilello, Acta Metall. Mater. **43**, 427 (1995).
[2]D. P. Adams, M. Vill, J. Tao, J. C. Bilello, and S. M. Yalisove, J. Appl. Phys. **74**, 1015 (1993).
[3]C. Montcalm, B. T. Sullivan, H. Pepin, J. A. Dobrowolski, and M. Sutton, Appl. Opt. **33**, 2057 (1994).
[4]J. H. Scofield, A. Duda, D. Albin, B. L. Ballard, and P. K. Predecki, Thin Solid Films **260**, 26 (1995).
[5]T. J. Vink and J. B. A. D. van Zon, J. Vac. Sci. Technol. A **9**, 124 (1991).
[6]T. J. Vink, M. A. J. Somers, J. L. C. Daams, and A. G. Dirks, J. Appl. Phys. **70**, 4301 (1991).
[7]R. W. Knoll and E. R. Bradley, Thin Solid Films **117**, 201 (1984).
[8]O. P. Karpenko, J. C. Bilello, and S. M. Yalisove, J. Appl. Phys. **76**, 4610 (1994).
[9]T. J. Vink, W. Walgrave, J. L. C. Daams, A. G. Dirks, M. A. J. Somers, and K. J. A. van der Aker, J. Appl. Phys. **74**, 988 (1993).
[10]D. S. Rickerby, A. M. Jones, and B. A. Bellamy, Surf. Coat. Technol. **37**, 111 (1989).
[11]D. P. Adams, L. J. Parfitt, S. M. Yalisove, J. C. Bilello, and Z. U. Rek, Thin Solid Films **266**, 52 (1995).
[12]W. C. Marra, P. Eisenberger, and A. Y. Cho, J. Appl. Phys. **50**, 6927 (1979).
[13]P. Eisenberger and W. C. Marra, Phys. Rev. Lett. **46**, 1081 (1981).
[14]P. H. Fouss and S. Brennan, Annu. Rev. Mater. Sci. **20**, 365 (1990).
[15]W. D. Nix, Metall. Trans. A **20**, 2217 (1989).
[16]J. D. Finegan and R. W. Hoffman, *Transactions of the Eigth National Vacuum Symposium* (Pergamon, New York, 1961), p. 935.
[17]P. A. Flinn, Mater. Res. Soc. Symp. Proc. **130**, 41 (1989).
[18]M. Renninger, Phys. Lett. **1**, 104 (1962).
[19]M. Renninger, Z. Phys. **19**, 20 (1965).
[20]M. Renninger, Z. Naturforsch. **160**, 1110 (1961).
[21]C. L. Kuo, P. E. Vanier, and J. C. Bilello, J. Appl. Phys. **55**, 375 (1984).
[22]G. G. Stoney, Proc. R. Soc. London Ser. A **82**, 172 (1909).
[23]D. W. Hoffman, in *Physics of Thin Films*, edited by G. Haas and R. E. Thun (Academic, New York, 1965), Vol. 3, p. 211.
[24]J. Tao, L. H. Lee, and J. C. Bilello, J. Electron. Mater. **20**, 819 (1991).
[25]I. C. Noyan and J. B. Cohen, *Residual Stress and Stress Relaxation*, Sagamore Army Materials Research Conference Proceedings (Plenum, New York, 1982), pp. 1–17.
[26]H. Dölle and V. Hauk, Z. Metallkd. **68**, 728 (1977).
[27]I. C. Noyan and J. B. Cohen, *Residual Stress Measurement by Diffraction and Interpretation* (Springer, New York, 1987), pp. 117–163.
[28]S. G. Malhotra, Z. U. Rek, S. M. Yalisove, and J. C. Bilello, J. Appl. Phys. **79**, 6872 (1996).
[29]C. J. Shute and J. B. Cohen, J. Appl. Phys. **70**, 2104 (1991).
[30]L. G. Parratt, Phys. Rev. **95**, 359 (1954).
[31]L. G. Schultz, J. Appl. Phys. **20**, 1030 (1949).
[32]T. Imura, S. Weissmann, and J. J. Slade, Jr., Acta Crystallogr. **15**, 786 (1962).
[33]J. F. Nye, *Physical Properties of Crystals* (Oxford Univeristy Press, Oxford, 1985).
[34]G. E. Deiter, *Mechanical Metallurgy* (McGraw–Hill, New York, 1961), p. 39.
[35]S. M. Foiles, Phys. Rev. B **48**, 4287 (1993).
[36]J. E. Sanchez and E. Arzt, Scr. Metall. Mater. **27**, 285 (1992).

[37]C. V. Thompson, Scr. Metall. Mater. **28**, 167 (1993).
[38]D. J. Srolovitz, J. Vac. Sci. Technol. A **4**, 2925 (1986).
[39]C. V. Thompson, Annu. Rev. Mater. Sci. **20**, 245 (1990).
[40]M. F. Toney and S. Brennan, Phys. Rev. B **39**, 7963 (1989).
[41]B. Ballard, X. Zhu, P. Predecki, and D. Braski, *Proceedings of the Fourth International Conference on Residual Stresses* (Society of Experimental Mechanics, Bethel, CT, 1994), p. 1133.
[42]T. Yamaguchi and R. Miyagawa, Jpn. J. Appl. Phys. **30**, 2069 (1991).
[43]A. G. Blachman, Met. Trans. **2**, 699 (1971).
[44]T. T. Bardin, J. G. Pronko, R. C. Budhani, J. S. Lin, and R. F. Bunshah, Thin Solid Films **165**, 243 (1988).
[45]P. Bosland, J. Danroc, R. Gillet, and L. Lombard, Thin Solid Films **166**, 309 (1988).
[46]J. A. Thornton and D. W. Hoffman, Thin Solid Films **171**, 5 (1989).
[47]M. F. Doerner and S. Brennan, J. Appl. Phys. **63**, 126 (1988).
[48]R. Venkatraman, P. R. Besser, J. C. Bravman, and S. Brennan, J. Mater. Res. **9**, 328 (1994).
[49]P. R. Besser, S. Brennan, and J. C. Bravman, J. Mater. Res. **9**, 13 (1994).
[50]L. J. Martínez-Miranda, J. J. Santiago-Avilés, W. R. Graham, P. A. Heiney, and M. P. Siegal, J. Mater. Res. **9**, 1434 (1994).
[51]D. A. Witte, R. A. Winholtz, and S. P. Neal, *Advances in X-Ray Analysis* (Plenum, New York, 1994), Vol. 37, pp. 265–277.